Published in final edited form as:
Cell Signal. 2015 March ; 27(3): 716–726. doi:10.1016/j.cellsig.2014.11.006.

Cannabinoid Receptor Interacting Protein (CRIP1a) attenuates CB_1R signaling in neuronal cells

Lawrence C. Blume[#1], **Khalil Eldeeb**[#1], **Caroline E. Bass**[1], **Dana E. Selley**[2], and **Allyn C. Howlett**[1]

[1]Department of Physiology and Pharmacology, Wake Forest University Health Sciences, Winston-Salem, NC 27157 USA

[2]Department of Pharmacology and Toxicology, Virginia Commonwealth University, Richmond, VA 23298 USA

[#] These authors contributed equally to this work.

Abstract

CB_1 cannabinoid receptors (CB_1R) are one of the most abundantly expressed G protein coupled receptors (GPCR) in the CNS and regulate diverse neuronal functions. The identification of GPCR interacting proteins has provided additional insight into the fine-tuning and regulation of numerous GPCRs. The Cannabinoid Receptor Interacting Protein 1a (CRIP1a) binds to the distal carboxy terminus of CB_1R, and has been shown to alter CB_1R-mediated neuronal function [1]. The mechanisms by which CRIP1a regulates CB_1R activity have not yet been identified; therefore the focus of this investigation is to examine the cellular effects of CRIP1a on CB_1R signaling using neuronal N18TG2 cells stably transfected with CRIP1a over-expressing and CRIP1a knockdown constructs. Modulation of endogenous CRIP1a expression did not alter total levels of CB_1R, ERK, or forskolin-activated adenylyl cyclase activity. When compared to WT cells, CRIP1a over-expression reduced basal phosphoERK levels, whereas depletion of CRIP1a augmented basal phosphoERK levels. Stimulation of phosphoERK by the CB_1R agonists WIN55212-2, CP55940 or methanandamide was unaltered in CRIP1a over-expressing clones compared with WT. However, CRIP1a knockdown clones exhibited enhanced ERK phosphorylation efficacy in response to CP55940. In addition, CRIP1a knockdown clones displayed a leftward shift in CP55940-mediated inhibition of forskolin-stimulated cAMP accumulation. CB_1R-mediated G_{i3} and G_o activation by CP99540 was attenuated by CRIP1a over-expression, but robustly enhanced in cells depleted of CRIP1a. Conversely, CP55940-mediated G_{i1} and G_{i2} activation was significant enhanced in cells over-expressing CRIP1a, but not in cells deficient of CRIP1a. These studies suggest a mechanism by which endogenous levels of CRIP1a modulate CB_1R-mediated signal transduction by facilitating a $G_{i/o}$-protein subtype preference for

To whom correspondence should be addressed: Allyn C. Howlett, Department of Physiology and Pharmacology, Wake Forest University Health Sciences, One Medical Center Blvd., Winston-Salem, NC 27157 USA. ahowlett@wakehealth.edu.

The authors declare no conflicts of interest.

G_{i1} and G_{i2}, accompanied by an overall suppression of G-protein-mediated signaling in neuronal cells.

Keywords

CB_1 receptor; CRIP1a; cAMP; ERK1/2; G protein; cell proliferation

1. Introduction

The CB_1 cannabinoid receptor (CB_1R) belongs to the class A rhodopsin-like G protein coupled receptor (GPCR) family. CB_1Rs display highest expression in the nervous systems [2-4], where they have been implicated in numerous physiological processes, including but not limited to energy balance, neuroprotection, pain, and cellular differentiation and proliferation [5]. Based on the location and function of CB_1Rs in the CNS, it is no surprise that CB_1Rs provide a potentially promising therapeutic target for a diverse number of diseases and disorders [6]; however, the clinical utility and success of CB_1R therapeutic agents has been impeded as a result of untoward side-effect profiles.

CB_1R signaling is mediated by pertussis toxin-sensitive $G_{i/o}$ proteins, and leads to inhibition of adenylyl cyclase (AC), regulation of ion channels, induction of immediate early gene expression, and activation of members of the mitogen-activated protein kinase (MAPK) family including extra-cellular regulated kinase 1/2 (ERK1/2) [7]. Studies using peptides mimicking specific regions of CB_1R's C-terminus or intracellular loop 3 have demonstrated a preference in binding of specific G proteins to different regions of CB_1R. $G\alpha_{i1}$ and $G\alpha_{i2}$ have been reported to interact with the third intracellular loop of CB_1R [8,9], whereas $G\alpha_{i3}$ and $G\alpha_o$ primarily interact with the juxtamembrane C-tail domain [8] of CB_1R. Additionally, specificity in G protein activation appears to occur in a ligand-dependent manner [10], suggesting that upon binding, CB_1R ligands can induce differences in receptor conformational changes, which can lead to the coupling and activation of specific G protein subtypes.

The GPCR C-terminal tail is a major site for protein-protein interactions, and although G protein binding is a key component in GPCR signaling, it is now well appreciated that other modulatory proteins are involved in receptor activity-dependent and G protein selective signaling [11,12]. The cannabinoid receptor interacting protein (CRIP1a), which binds to the distal C-terminal tail of CB_1R, was initially characterized for its ability to reverse CB_1R-mediated tonic inhibition of Ca^{2+} channels in superior cervical ganglion neurons [1]. Studies using a cell culture model of glutamate neurotoxicity in primary neuronal cortical neurons, showed that lentiviral over-expression of CRIP1a reversed CB_1R-mediated neuroprotection from an agonist- to antagonist-driven mechanism [13]. However, the underlying mechanism responsible for this modification of CB_1R ligand-mediated neuroprotection is unknown.

To explore the emerging roles of CRIP1a in regulating CB_1R, our laboratory developed CRIP1a gain and loss of function transgenic neuronal clones, and reported preliminary observations of alterations in agonist-promoted CB_1R activation and internalization by CRIP1a [14,15]. In the present study, we determined the effect of CRIP1a on CB_1R

signaling and the associated downstream consequences on cellular function. Both CRIP1a over-expression and RNA interference-induced CRIP1a knockdown were examined in stably-transfected clones of the N18TG2 neuronal cell line, which endogenously expresses both CB_1R and CRIP1a. The focus was on CB_1R-$G\alpha_{i/o}$-mediated inhibition of cAMP production and $G\beta\gamma$-mediated MAPK activation. Herein we demonstrate that CRIP1a functions as a negative modulator of CB_1R cellular signaling, as depletion of CRIP1a increased the interaction with G_{i3} and G_o subtypes, increased the potency of CB_1R agonists to inhibit forskolin-stimulated cAMP accumulation, and enhanced the efficacy of CB_1R agonist-stimulated ERK phosphorylation. These studies suggest a role for CRIP1a in CB_1R signaling and modulation of agonist-mediated G protein coupling.

2. Materials and Methods

2.1. Cell culture and generation of stable neuronal CRIP1a transgenic clones

N18TG2 neuroblastoma cells and stable clones were cultured and maintained in complete media containing Dulbecco's Modified Eagle's Medium (DMEM):Ham's F-12 (1:1) with GlutaMax, sodium bicarbonate, and pyridoxine-HCl, supplemented with penicillin (100 units/ml) and streptomycin (100 μg/ml) (Gibco Life Technologies, Gaithersburg, MD, USA) and 10% heat-inactivated bovine serum (JRH Biosciences, Lenexa, KS, USA), and incubated at 37°C in a humidified atmosphere containing 95% air and 5% carbon dioxide.

For creation of stable CRIP1a over-expressing and knockdown clones, mouse N18TG2 cells (passage 23) were grown to 90% confluency and then transfected with either a pcDNA3.1-CRIP1a mouse cDNA plasmid for over-expression, or an siRNA-CRIP1a plasmid for knockdown, using Lipofectamine 2000 (Life Technologies, Grand Island, NY, USA). The siRNA-CRIP1a target sequences were selected by the siRNA target finder program on the GenScript website (https://www.genscript.com/ssl-bin/app/rnai) using the mRNA sequence NM_029861 (mouse Cnrp1 mRNA). Two different siRNA-CRIP1a transcripts were created (pRNATin-H1.2-GGATCCCATTTCCATT GGT GGTGTC CTTACTCGAGA; pRNATin-H1.2-GGATCCCATTACCA CAAGCGAGAC CATTAC TCGAGA), and each was individually tested for knockdown efficiency. An empty pcDNA3.1 or pRNATin-H1.2 vector was used as a Control for CRIP1a over-expression or siRNA-CRIP1a knockdown, respectively. To generate stable CRIP1a N18TG2 cell lines, G418-resistent single colonies were isolated and expanded in selection media containing 600 μg/ml G418 (Gibco Life Technologies, Gaithersburg, MD, USA), and were maintained in 200 μg/ml G418.

CRIP1a and CB_1R expression in transgenic clones was determined using quantitative real-time polymerase chain reaction (qPCR). N18TG2 wild-type (WT) and CRIP1a over-expressing (XS) and knockdown (KD) clones were grown to 90% confluency and harvested with PBS-EDTA (2.7 mM KCl, 138 mM NaCl, 10.4 mM glucose, 1.5 mM KH_2PO_4, 8 mM Na_2HPO_4, 0.625 mM EDTA, pH 7.4). Cells were pelleted at 1,000 × g at 4°C for 5 min and total RNA was isolated and purified using an RNeasy Mini Kit (Qiagen, Germantown, MD, USA). RNA quantification and purity was determined with a 260/280 ≥ 2.0 and 260/230 ≥ 1.8 absorbance ratio (NanoDrop 1000 Spectrophotometer, Thermo Scientific). Total RNA (1 μg) was reverse transcribed into cDNA using a High-Capacity cDNA Archive Kit (Applied Biosystems, Grand Island, NY, USA). Real-time qPCR was performed in triplicate for each

sample using TaqMan Universal PCR Master Mix and specific TaqMan primer-probe assay sets (Applied Biosystems, Grand Island, NY, USA) for the following genes: 18s ribosomal RNA, neuron-specific enolase 2 (eno2), CB_1 cannabinoid receptor (cnr1), and CRIP1a (cnrip1). Data were analyzed using the ΔΔCT method and eno2 served as the reference standard.

Because N18TG2 cells can produce 2-arachidonoylglycerol (2-AG) [16], cells at 90% confluency were serum-starved (18 h) and pretreated with the diacylglycerol lipase (DAGL) inhibitor THL (1 μM, 2 h) prior to stimulation with cannabinoid agonists. For drug treatment assays, an aliquot of cannabinoid drug stock (stored at −20°C as 10 mM solutions in ethanol) or ethanol (control) were air-dried under sterile conditions in trimethylsilyl-coated glass test tubes, resuspended in100 volumes of 5 mg/ml fatty acid-free bovine serum albumin (BSA) and serially diluted before being added to cells. Where indicated, N18TG2 WT or CRIP1a XS or CRIP1a KD cells were pretreated with receptor antagonists or other inhibitors prior to addition of CB_1R agonists.

2.2. Whole cell lysates and NP-40-soluble and insoluble membrane fractions

For whole cell protein analyses of N18TG2 clones, cells were harvested with PBS-EDTA and cell pellets were resuspended for 30 min on ice in cold Lysis Buffer (50 mM Tris-HCl, pH 7.2, 2 mM EDTA, 0.35 mM NP-40, and a protease inhibitor cocktail (EMD Biosciences, La Jolla, CA, USA). Whole cell detergent lysates were centrifuged at 2,500 × g at 4°C for 5 min to remove debris, and the supernatants were collected for protein determinations (BCA assay, Pierce, Rockford, IL, USA).

To prepare detergent-solubilized membrane fractions, cells grown to sub-confluency (~80%) were harvested with PBS-EDTA, and cell pellets were resuspended for 20 min on ice in cold hypotonic swelling buffer (20 mM HEPES (pH 7.4), 10 mM KCl, 1.5 mM $MgCl_2$, 1 mM EDTA, 1 mM EGTA, 1 mM dithiothreitol (DTT) and a protease inhibitor cocktail (EMD Biosciences, La Jolla, CA, USA). Cells were subjected to 20 strokes with a dounce homogenizer, and homogenates were centrifuged at 1,000 × g for 10 min at 4°C to remove cellular debris and unbroken cells. Supernatants were centrifuged at 40,000 × g for 1h at 4°C, and the membrane pellet was resuspended with a 25 G needle in ice cold Lysis Buffer, and incubated on ice for 20 min. NP-40-solubilized membranes were centrifuged at 2,500 × g for 10 min at 4°C, and NP-40-soluble membranes (supernatant) were used to determine protein using the BCA assay. The NP-40-resistant fractions (pellets) were resuspended in the same volume of Laemmli buffer to allow for volume-to-volume equivalence in the Western blot analysis.

2.3. Immunoblot analysis

Samples were denatured and reduced in Laemmli sample buffer (62.5 mM Tris-HCl, pH 6.8, 2% SDS, 10% glycerol, 0.002% bromophenol blue, 710 mM β-mercaptoethanol; 65 °C for 10 min), and then resolved on 4-20% gradient SDS-PAGE gels (Bio-Rad, Hercules, CA, USA) at 150 volts for 1 h at 21-23°C. Proteins were transferred to nitrocellulose membranes in Towbin's buffer at 85 volts for 45 min at 4°C using a BioRad Trans-Blot Cell with an ice pack. Blots were rinsed for 5 min with phosphate-buffered saline (PBS: 1.5 mM KH_2PO_4,

2.7 mM KCl, 8 mM Na_2HPO_4, 150 mM NaCl, pH 7.4), blocked for 60 min with blocking buffer (LI-COR Biosciences, Lincoln, NE, USA), and then incubated with primary antibodies at 4°C for 18 h: CB_1R (1:750), CRIP1a D20 (1:500) [17], CRIP1a K-12 (1:500), β-actin (1:600), β-arrestin-1/2 (1:500), caveolin-1 (1:500), Na^+/K^+-ATPase (1:500) (Santa Cruz Biotechnology, Paso Robles, CA, USA). Blots were washed four times with PBST (PBS containing 0.1% Tween-20), incubated with an appropriate IRDye-conjugated secondary antibody (1:10,000) for 1 h at 21-23°C, and washed three times with PBST followed by one wash with PBS. Bands on immunoblots were imaged and quantified by densitometry using Odyssey Infrared Imaging System software (LI-COR Biosciences, Lincoln, NE, USA).

2.4. Immunocytochemistry determination of protein levels

Total CB_1R, CRIP1a, ERK1/2, and phosphoERK1/2 protein levels were quantified using a 96-well format "In-cell-Western" immunocytochemistry technique [18]. N18TG2 WT, Control vector, CRIP1a XS and CRIP1a KD cells were seeded at a density of 30,000 cells per well, grown until 90% confluent, serum-starved for 16 h and pretreated with 1 μM THL for 2 h prior to stimulation with cannabinoid agonists. Cells were treated with vehicle, 10 nM CP55940, 10 nM WIN55212-2, 10 nM mAEA (R-(+)-methanandamide), or 10 nM SR141716A at 37°C for the indicated times. Drug-containing media was immediately poured off, and plates were placed on ice. Cells were fixed with ice-cold 4% phosphate-buffered formalin (1.5 mM KH_2PO_4, 2.7 mM KCl, 8 mM Na_2HPO_4, 150 mM NaCl; 4% formaldehyde (v/v), pH 7.4), incubated for 15 min at 21-23°C, permeabilized with PBST (PBS containing 0.3% triton X-100) for 15 min, and blocked for 90 min in Odyssey blocking buffer (LI-COR Biosciences, Lincoln, NE, USA). Plates were incubated with gentle rocking at 4°C for 18 h with a primary antibody: CB_1R (1:800), CRIP1a D20 (1:500) [17], CRIP1a K-12 (1:500), GAPDH (1:500), ERK2 (1:500), phosphoERK (Thr 202, Tyr 204; 1:300) (Santa Cruz Biotechnology, Paso Robles, CA, USA). Plates were washed in PBST, and incubated simultaneously for 1 h with a secondary IRDye 800CW donkey anti-goat (1:800), IRDye 800CW goat anti-rabbit (1:800), or IRDye 800CW donkey anti-mouse (1:800) (LI-COR Biosciences, Lincoln, NE, USA). The nuclear stain DRAQ5 (1:5,000) (Cell Signaling, Danvers, MA, USA) was used to normalize for well-to-well variations in cell density. Plates were washed four times with PBST, and immunofluorescence was imaged using the LI-COR Odyssey (169 μ resolution, 5 sensitivity, 4.01235 mm offset, medium quality). Basal expression for CB_1R, CRIP1a, and phosphoERK was calculated as the ratio of immunoreactive CB_1R:DRAQ5, CRIP1a:DRAQ5, or phosphoERK1/2:total ERK, respectively. CP55940-stimulated log dose response curves for CB_1R-mediated phosphoERK were determined as the ratio of phosphoERK1/2:total ERK, and then ratios were quantified as percent change relative to basal expressed as 100% for WT cells. Changes in CB_1R, CRIP1a, ERK1/2, and phosphoERK protein expression were analyzed using Microsoft Excel and GraphPad Prism 6 software.

For determination of CB_1R cell surface density a 96-well format "On-cell-Western" immunocytochemistry technique was utilized. Cells were plated and grown until 90% confluent, serum-starved for 16 h, and then treated for 2 h with 1 μM THL to attenuate the production of 2-AG. Cells were fixed with ice-cold 1.2% phosphate-buffered formalin (1.5

mM KH_2PO_4, 2.7 mM KCl, 8 mM Na_2HPO_4, 150 mM NaCl; 1.2% formaldehyde (v/v), pH 7.4) and incubated for 15 min at 21-23°C, with elimination of the permeabilization step. To determine a concentration of formaldehyde capable of fixing cells to the micro-well plate without altering plasma membrane permeability, the effects of various concentrations of formaldehyde were assessed. LAMP2, a luminal endosomal marker, was used as a positive control for determining the extent of cell permeabilization (Fig. 2A). Plates were then subjected to the identical parameters previously described for the "In-cell-Western" assay.

2.5. cAMP assay

The assay was performed as previously described [19], but modified for a multiwell plate. Briefly, N18TG2 WT, Control vector, CRIP1a XS, and CRIP1a knockdown cells were seeded in a 24-well plate at a density of 120,000 cells per well and grown to 90% confluence. Cell media was removed and washed with warm (37°C) Physiologic Saline Solution-HEPES-BSA (145 mM NaCl, 10 mM glucose, 5 mM KCl, 1 mM $MgSO_4$, 10 mM HEPES, 0.5mg/ml BSA, pH7.4) then incubated with 100 μM IBMX and 100 μM rolpiram (Caymen Chemical, Ann Arbor, MI, USA) plus either vehicle or varying concentrations (1, 3, 10, 30, 100, 300 nM) of mAEA, WIN55212-2, or CP55940 for 15 min. The assay was initiated by adding 1 μM forskolin (Tocris Bioscience, Minneapolis, MN, USA) for 4 min. The reaction was terminated by dropping the pH with 50 mM NaAcetate (pH 4.5) and heating to 90°C. Cells were disrupted by a freeze-thaw cycle, sedimented, and cell-free supernatants were collected and stored at −80°C until assayed. cAMP was quantitated using a radioligand displacement assay based upon [^{3}H]-cAMP (PerkinElmer, Billerica, MA, USA) binding to protein kinase A regulatory proteins [20]. Bound proteins were aggregated with 30% polyethelene glycol 8000 (PEG 8000), harvested on a UniFilter and quantitated using a Top Count scintillation counter (Pac PerkinElmer, Billerica, MA, USA). The data for each assay were normalized to forskolin-stimulated cAMP accumulation as 100%, and statistical differences were determined by two-way analysis of variance (ANOVA) followed by Bonferroni post-hoc analysis.

2.6. GTPγS-Binding Scintillation Proximity Assay

N18TG2 clones were subjected to GTPγS-binding reactions in triplicate in 96-well Opti-plates (PerkinElmer, Waltham, MA, USA), as previously described [21]. Briefly cell membranes were collected as described in section 2.2; however, following the 40,000 × g centrifugation cell pellets were homogenized in TME buffer (20 mM Tris Cl_2; 5 mM $MgCl_2$; 1 mM Tris-EDTA; 1 mM DTT; pH 7.4), subjected to BCA analysis for total protein concentration, and then stored at −80°C. The assay was initiated by the addition of cell membranes (5 μg protein) to the assay buffer (20 mM NaHepes, pH 7.4, 100 mM NaCl, 5 mM $MgCl_2$, and 1 mM DTT) containing 500 pM [^{35}S]GTPγS (PerkinElmer, Billerica, MA, USA), 10 μM GDP and cannabinoid ligands for 1 h at 30°C. Membranes were then placed on ice (4°C), lysed with 3% IGEPAL CA-630 for 30 min, incubated with primary antibodies anti-$G\alpha_o$, anti-$G\alpha_{i1}$, anti-$G\alpha_{i2}$, or anti-$G\alpha_{i3}$ (Santa Cruz Biotechnology, Paso Robles, CA, USA) for 1 h. Scintillation proximity assay beads coated with the anti-rabbit or anti-mouse IgG (PerkinElmer, Billerica, MA, USA) were added for 30 min, and the plates were then centrifuged at 1,000 × g for 5 min. The radioactivity was detected on a Top-Count scintillation counter (PerkinElmer, Billerica, MA, USA). The non-specific binding was

determined in the presence of 10 μM GTPγS. Basal values were in the absence of the ligands. Specific GTPγS-binding (counts per minute; CPM) was determined by subtracting non-specific activity. Agonist-stimulated values were transformed to "percent over basal" [% = (stimulated-basal)/(basal)*100]. Statistical differences in GTP-binding parameters were determined using two-way ANOVA and Bonferroni post-hoc analysis.

2.7. Statistical analysis

Graphs and statistical analyses were generated using GraphPad Prism 6 software (La Jolla, CA, USA). Data were compared and analyzed using the unpaired Student's t-test, or as described above. For dose-response experiments EC_{50} values were determined by non-linear regression analysis. All data are expressed as the mean ± SEM, and were considered significant when the p value ≤ 0.05.

3. Results

3.1. CRIP1a influences CB_1R cell surface equilibrium but not mRNA or total protein levels

In order to better understand the cellular mechanisms involved in the regulation of CB_1R by CRIP1a, we developed stable neuronal transgenic CRIP1a over-expressing (XS) and knockdown (KD) clones in the N18TG2 cell line. Based on their CRIP1a mRNA and protein expression, two different CRIP1a XS and KD clones were selected for the present investigation. CRIP1a XS clones 1 and 5 express CRIP1a:CB_1R mRNA levels that are 12:1 (XS 1) and 7:1 (XS 5), compared with a 1:7 ratio in WT cells (Fig. 1A). qPCR analysis of N18TG2 CRIP1a knockdown clones showed that these cells have a significant depletion in the mRNA levels of CRIP1a (KD 2C: 61±6%; KD 2F: 70±6%) relative to Control and N18TG2 WT cells (Fig. 1C). N18TG2 cells stably transfected with either an empty pcDNA3.1 expression plasmid (XS Control) or the siRNA expression vector pRNATin-H1.2 (KD Control) did not show any significant changes in the mRNA levels of CRIP1a. Western blot analysis using a CRIP1a antibody, recognizing an internal (D20) or a C-terminus (data not shown) epitope, confirmed that these transgenic CRIP1a clones have significant alterations in CRIP1a protein levels, relative to WT controls (Fig. 1B and D). To determine whether alterations in CRIP1a expression could change CB_1R mRNA or total protein levels we performed qPCR and immunoblotting in CRIP1a XS and KD clones. Results from CB_1R gene expression experiments revealed that over-expression (Fig. 1E) and knockdown (Fig. 1G) of CRIP1a failed to alter CB_1R mRNA levels. Furthermore, comparison of Western immunoblot band densities between WT and CRIP1a XS (Fig. 1F) or KD (Fig. 1H) cells show that variation in cellular CRIP1a levels did not influence total CB_1R protein levels. These findings support work from several recent publications using stable and transient over-expression of CRIP1a, which indicated that CRIP1a had no effect on total CB_1R protein expression [1,13,17].

We next investigated the influence of CRIP1a in regulation of CB_1R cell surface density. Endogenous 2-AG has been reported to modulate CB_1R internalization [22,23,24]. Therefore, to diminish contributions of endocannabinoid tone, cells were serum-starved for 16 h to remove any endocannabinoids that may be present in the serum [25], and then treated with the diacylglycerol lipase inhibitor THL for 2 h to attenuate the production of 2-

AG [26]. Pretreatment with THL did not change the total or cell surface levels of CB_1R (data not shown). Cells were fixed with a concentration of formaldehyde (1.2%) that was capable of maintaining cell attachment, but not cellular permeabilization, as determined via immunodetection of the intracellular lysosome-associated membrane protein 2 (Fig. 2A). Utilizing an antibody directed at the N-terminal domain of CB_1R, we observed that CB_1R cell surface immunoreactivity was significantly reduced in cells that stably over-expressed CRIP1a (XS 1: −29±6%; XS 5: −24±6%) (Fig. 2B). In contrast, knockdown of CRIP1a led to an augmentation of CB_1R surface density (KD 2C: 14±4%; KD 2F: 22±5%) (Fig. 2B). A 2 h pre-treatment with the protein synthesis inhibitor cycloheximide (50 μM) failed to alter the observed effects on CB_1R plasma membrane density in CRIP1a XS or KD cells, suggesting that CRIP1a does not change the rates of CB_1R de novo synthesis and translocation to the plasma membrane (data not shown). We did not observe any significant differences in CB_1R surface immunoreactivity between WT and empty vector Control cells (Fig. 2B).

Although CRIP1a is a soluble protein, its co-localization with CB_1R at the plasma membrane has been reported in HEK293 cells [1]. Previous work in human breast cancer MDA-MB-231 cells using cholesterol-depleting agents suggested that disruption of lipid rafts impairs autocrine signaling of CB_1R's [27]. Furthermore, in C6 glioma cells microscopy analysis revealed a strong association between CB_1R and caveolin-1, and a requirement for lipid rafts in the regulation of CB_1R signaling and internal trafficking [28,29]. We therefore investigated whether CRIP1a over-expression or knockdown might sequester CB_1R membrane proteins into different plasma membrane microdomains (i.e. caveolar lipid rafts), by preparing NP-40 soluble and NP-40-resistant membrane fractions for Western blotting. In Fig. 2C the NP-40 soluble fraction contains the vast majority of the membrane-associated CRIP1a and CB_1R. It is important to note that both over-expression and knockdown of CRIP1a can be observed in the NP-40-soluble membrane fractions. Membrane lipid raft fractions, defined by their NP-40-resistance, the presence of caveolin-1, and deficiency of Na^+K^+-ATPase, contained much less CB_1R and CRIP1a relative to NP-40 soluble fractions (Fig. 2D). Overall, no discernable differences in the ratios of CRIP1a:CB_1R were detected between caveolar-rich and caveolar-deficient membrane fractions, indicating that the CB_1R distribution in CRIP1a-modified clones is not reflected by a disparate partitioning of CRIP1a or CB_1R into plasma membrane microdomains.

3.2. CB_1R-mediated constitutive as well as agonist-stimulated ERK phosphorylation is modulated by CRIP1a

Initial observations of cellular signaling regulation by CRIP1a indicated that exogenously expressed CRIP1a suppressed the constitutive activity of CB_1R to release Gβγ and inhibit Ca^{2+} channels [1]. We utilized the In-cell-Western immunocytochemical technique to assess CRIP1a-related changes in phosphoERK1/2 (Thr202, Tyr204) after blocking endogenous 2-AG production. Under basal conditions (non-ligand dependent), levels of ERK1/2 phosphorylation were significantly reduced in CRIP1a XS clones (XS 1, −16±5%; XS 5, −20±6%) compared to WT cells (Fig. 3A). In contrast, knockdown of CRIP1a augmented basal phosphoERK1/2 levels (KD 2C, 13±5%; KD 2F, 27±8%). A 5-min treatment with the CB_1 antagonist/inverse agonist SR141716A (10 nM) reduced basal levels of

phosphoERK1/2 in WT and Control cells, consistent with the definition of CB_1R-mediated constitutive signaling (WT, −17±4%; Control, −20±6%) (Fig. 3B). However, CRIP1a XS clones were insensitive to the CB_1R inverse agonist SR141716A (10 nM), suggesting the absence of non-ligand dependent constitutive CB_1R activity (Fig. 3B). In contrast, KD cells deficient in CRIP1a displayed an enhancement in SR141716A-reversible constitutive phosphoERK1/2 compared with WT and Control cells.

As seen in Fig. 4, a 5-min incubation with the CB_1 full agonist WIN55212-2 or CP55940 resulted in a robust enhancement in phosphoERK1/2 levels in WT cells (WIN55212-2, 36±5%; CP55940, 45±6%). mAEA, a CB_1R partial agonist, modestly increased (12±2%) ERK phosphorylation to a level that was ~30% of the response observed with a CB_1R full agonist (Fig. 4). Under these same agonist-stimulated conditions, no differences were observed between Control cells and cells over-expressing CRIP1a (Fig. 4A). However, depletion of CRIP1a caused a significant increase in CP55940-stimulated maximal ERK1/2 phosphorylation when compared with WT cells (CP55940: KD2C, 63±8%; KD2F, 59±4%) (Fig. 4B). This increase was ligand-selective, as it was not observed with WIN55212-2 or mAEA.

To identify the mechanism for the influence of CRIP1a on agonist-stimulated activity, we examined CP55940 concentration-response relationships. In WT and Control cells, CP55940 treatment led to a dose-dependent increase in phosphoERK1/2 levels that peaked at 10 nM (E_{max}: WT = 57±6%; Control = 55±7%) (Fig. 5A and B). This effect was mediated by the CB_1R, as it was completely abolished by concurrent treatment with 1 μM SR141716A (Fig. 5C and D). CRIP1a XS cells exhibited a comparable concentration-dependent increase in CP55940-stimulated phosphoERK1/2, which was completely blocked by SR141716A (Fig. 5A and C). In contrast, CRIP1a KD cells showed an enhancement in maximal CP55940-stimulated ERK1/2 phosphorylation (10 nM: KD2C = 68±4%; KD2F = 73±5%: 100 nM: KD2C = 58±5%; KD2F = 62±6%) when compared with WT (10 nM: 55±6%) (Fig. 5B). A two-way ANOVA revealed a significant main effect of both the CP55940 treatment ($F_{4,90}$=149.5, p<0.01), and the cell line ($F_{5,90}$=6.56, p<0.01). *Post-hoc* Bonferroni analysis indicated that CRIP1a KD cells exhibited an increase in phosphoERK1/2 levels at the 10 and 100 nM concentrations as compared to WT and Control cells. Pretreatment with SR141716A eliminated CP55940-stimulated phosphoERK1/2, confirming that a CB_1R-mediated signaling mechanism was involved (Fig. 5D).

WT and CRIP1a-XS and KD cells exposed to 10 nM CP55940 showed a rapid increase in the levels of phosphoERK1/2 within 5 min, before declining and reaching a sustained plateau level just above basal (Fig. 6A and B). This 3-phase response is in alignment with a previously published report [30]. No significant difference between WT and CRIP1a-XS cells was observed. In Fig. 6B, CRIP1a KD cells displayed a time-dependent enhancement in CP55940-stimulated phosphoERK1/2 levels. A two-way ANOVA revealed a significant main effect of time ($F_{12,78}$=35.6, p<0.05), and the cell line ($F_{5,90}$=9.8, p<0.05). *Post-hoc* Bonferroni analysis indicated an increase in CP55940-stimulated phosphoERK1/2 levels at 5, 10, and 15 min in CRIP1a KD cells compared to WT and Control (data not shown) cells. Preincubation with the dynamin inhibitor Dynasore completely blocked CP55940-stimulated phosphorylation of ERK1/2 by CB_1R (Fig. 6A and B), suggesting that for WT, CRIP1a-XS

and KD clones, agonist-stimulated ERK phosphorylation is an internalization-dependent signaling process.

3.3. CB_1R-mediated inhibition of cAMP accumulation is potentiated by CRIP1a knockdown

To determine cAMP levels in intact N18TG2 cells, we treated cells with the adenylyl cyclase activator forskolin (1μM) in the presence or absence of CB_1R agonists for a maximum of 4 min (prior to heterologous desensitization). Comparisons indicated that basal levels of cAMP between WT, Control, CRIP1a XS, or CRIP1a KD clones were not significantly different (Fig. 7A). Additionally, forskolin was able to stimulate cAMP accumulation over vehicle to the same extent in all cell lines tested (Fig. 7A). However, CRIP1a clones did displayed changes in CB_1R-mediated regulation of cAMP accumulation, which occurred in an agonist selectivity manner. We observed a concentration-dependent attenuation in cAMP accumulation by the endogenous agonist analog mAEA, and this effect was not altered by differences in the expression of CRIP1a (Fig. 7B). Forskolin-stimulated cAMP was robustly inhibited by WIN55212-2 in a concentration-dependent manner in WT (EC_{50} = 3.7 nM, 95% CI [1.5, 5.3]) and Control cells (EC_{50} = 6.4 nM, 95% CI [5.2, 7.9]) (Fig. 7C). Over-expression of CRIP1a did not alter WIN5521-2-mediated inhibition of cAMP accumulation at any doses tested (EC_{50} = 4.7 nM, 95% CI [4.1, 7.5]) (Fig. 7C). Although not statistically significant, we observed a trend toward a leftward shift in the concentration-dependent inhibition of cAMP accumulation by WIN55212-2 in CRIP1a KD cells (EC_{50} = 1 nM, 95% CI [0.5, 2.3]). CRIP1a knockdown (EC_{50} = 0.2 nM, 95% CI [0.09, 2.5]), but not CRIP1a over-expression (EC_{50} = 1.6 nM, 95% CI [0.02, 2.9]), was able to dose-dependently enhance the attenuation of cAMP accumulation by treatment with CP55940, compared with WT cells (EC_{50} = 3.4 nM, 95% CI [0.9, 8.2]). A two-way ANOVA revealed a significant main effect of CP55940 concentration ($F_{9,114}$=3.9, p<0.05), and the cell line ($F_{3,114}$=4.3, p<0.05). These data reveal that depletion of CRIP1a increases the relative potency of CP55940 to induce CB_1R-mediated inhibition of cAMP accumulation of forskolin-stimulated cAMP formation. Together, these studies suggest that CRIP1a can function to negatively modulate CB_1R function in a ligand-specific manner.

3.4. CRIP1a modulates G protein selectivity of CB_1R signaling

Because coupling to both adenylyl cyclase and ERK phosphorylation is initiated by activation of pertussis toxin-sensitive $G_{i/o}$ proteins by the [31,32], we tested the effect of CRIP1a over-expression and knockdown on CB_1R agonist-promoted G protein activation. Using a scintillation proximity assay for [^{35}S]GTPγS-binding, we determined the coupling of CB_1R with different Gα subunits in cell membranes treated with either 100 nM CP55940 or SR141716A, or with CP55940 together with SR141716A. CP55940 stimulated [^{35}S]GTPγS binding to $G\alpha_{i3}$ in WT (79±18% over basal) and Control clones (62±21% over basal), which was absent during co-incubation with SR141716A (Fig. 8A), providing support for a CB_1R-mediated mechanism. SR141716A acted as an inverse agonist to reverse constitutive CB_1R-mediated $G\alpha_{i3}$ activation in WT (−41±6% relative to basal) and Control (−43±8%) cells, a finding that is consistent with the definition of constitutively active CB_1 receptors. Over-expression of CRIP1a attenuated CP55940-stimulated [^{35}S]GTPγS binding to $G\alpha_{i3}$ (10±12% over basal), whereas depletion of CRIP1a significantly increased CB_1R-mediated activation of $G\alpha_{i3}$ (103±22% over basal) (Fig. 8A). CRIP1a XS cells were

resistant to SR141716A-mediated attenuation of the $G\alpha_{i3}$ constitutive activation (Fig. 8A), whereas the inverse agonist response to SR141716A in CRIP1a KD cells (54±7% below basal) was similar to WT and Control cells. WT cell membranes treated with CP55940 showed a robust enhancement in [^{35}S]GTPγS binding to $G\alpha_o$ (49±9% over basal) (Fig. 8B). This agonist stimulation was blocked in CRIP1a XS cells (4±3% over basal), and significantly augmented in CRIP1a KD cells (79±21% over basal) (Fig. 8B). CP55940-promoted coupling between $G\alpha_o$ and CB_1R was attenuated by SR141716A in all cell lines. SR141716A alone decreased constitutive binding of [^{35}S]GTPγS to $G\alpha_o$ in WT (30±5% below basal) and Control cells (17±13% below basal) (Fig. 7B). However, over-expression of CRIP1a attenuated and knockdown of CRIP1a augmented (43±5% below basal) the inverse agonist response to SR141716A for $G\alpha_o$.

To test the idea that CRIP1a might alter G protein bias toward a $G_{i1/2}$ mechanism, we examined the ability of CP55940 to stimulate [^{35}S]GTPγS binding to $G\alpha_{i1}$ and $G\alpha_{i2}$. We observed no differences in the binding of $G\alpha_{i1}$ or $G\alpha_{i2}$ to CB_1R following CP55940-treatment in WT, Control or CRIP1a KD cells (Fig. 8C and D). However, a robust stimulation of [^{35}S]GTPγS binding to $G\alpha_{i1}$ (128±54% above basal) or $G\alpha_{i2}$ (753±316% above basal) occurred in response to CP55940 in CRIP1a XS cells (Fig. 8C). This response was reversed by co-incubation of CP55940 with SR141716A. No significant SR141716A-reversable constitutive activity was observed with these G_i proteins. Overall these experiments indicate that CRIP1a can disrupt CB_1R-$G_{i3/o}$ coupling, and can promote a switch to $G_{i1/2}$ coupling.

Discussion

In addition to direct stimulation of the receptor by agonists, signaling by CB_1R can be further modified by accessory proteins, such as β-arrestin, G protein Associated Sorting Proteins (GASP), and CRIP1a [11,12,15]. CRIP1a was initially characterized for its ability to bind to a segment of the distal C-terminal of the CB_1R [1]. Following that report, studies of retinal circuitry showed that CRIP1a could be found in amacrine cells, and in certain cone (but not rod) terminals [33]. The CB_1R-CRIP1a presynaptic co-localization was juxtaposed across from postsynaptic diacylglycerol lipase at photoreceptor/Type1 OFF cone-bipolar cell synapses. These findings suggest selectivity based upon limited co-expression (not all cells express both CB_1R and CRIP1a proteins concurrently), but also functional relevance in that both proteins are found in the presynaptic terminals close to the source of agonist ligand production. We previously provided evidence that experimental depletion of CB_1R by RNA interference in dorsal striatal neurons was associated with an increase in expression of CRIP1a [17]. This finding leads to speculation that a heterologous compensatory mechanism might be occurring in either the same or neighboring CB_1R-expressing neurons (note that both D1- and D2-dopamine receptor-expressing medium spiny neurons, as well as some interneuron types, express CB_1R in the dorsal striatum [34]). Although these studies lend support to the concept that the association of CRIP1a and CB_1R results in some functional dynamic, the nature of that function has not yet been established.

The initial function reported for CRIP1a was the ability of heterologously expressed CRIP1a to attenuate constitutive inhibition of N-type Ca^{2+} channels by exogenously expressed CB_1R

in superior cervical ganglion neurons [1]. Enthusiasm for this finding was tempered by the observation that there was no apparent change in agonist-induced inhibition of N-type Ca^{2+} channels [1]. Our laboratories decided to investigate the role of CRIP1a in CB_1R cellular signaling using a model neuronal cell line in which CB_1R function has been highly characterized [11]. This cell line exhibits many neuronal properties, including neuropeptide synthesis, cellular signaling responses to several neuropeptides, and the appearance of neurons (soma plus extensions) that can be quantified as a measure of neuronal differentiation in culture [35]. The N18TG2 cell endogenously expresses CRIP1a, which makes this cell a prototype for a neuron that co-expresses both CB_1R and CRIP1a such that functional interactions between these two proteins can be examined under natively expressed conditions. Therefore, we created both CRIP1a loss and gain of function clones in the N18TG2 cell line in order to understand the role of CRIP1a in regulating cellular signaling processes.

One pertinent observation from comparing CRIP1a cell clones with WT and appropriate empty-vector Controls that express endogenously relevant CRIP1a levels, is that the CB_1R levels at the plasma membrane are reduced in cells over-expressing CRIP1a, and increased in cells depleted of CRIP1a. These findings were determined using a quantitative On-cell-Western immunocytochemical assay that detects extracellular plasma membrane surface protein levels using an N-terminal epitope, as well as in the cell membrane fractions. This dys-equilibrium in plasma membrane receptor levels might suggest a role for CRIP1a in either chaperoning or delivery of CB_1R to the plasma membrane, and/or removal of CB_1R from the plasma membrane. Our data demonstrate that neither gene expression nor total cellular protein levels of CB_1R are altered by changing the level of CRIP1a expression, and that protein synthesis inhibition does not change CB_1R plasma membrane density in CRIP1a XS or KD cells. Using stable and transient over-expression of CRIP1a, other laboratories and us have shown that CRIP1a had no effect on total CB_1R protein expression using other models [1,13,17]. These findings suggest that plasma membrane CRIP1a localization is not dependent on CB_1R de novo synthesis. Alternatively, it is plausible that CRIP1a could influence the rates of CB_1R translocation to, or removal from the plasma membrane. CB_1R is required for presynaptic regulation of neurotransmitter release at the synapse [36]. To accommodate that function, kinetics of CB_1R plasma membrane localization at the soma appears to differ from those at the presynaptic terminals [22,37]. Of interest, constitutive internalization is a property of neuronal CB_1R [22,23], but whether it is driven as an autocrine or paracrine function of endocannabinoid tone has not been determined. Nevertheless, studies are underway in our laboratory to investigate the role of CRIP1a in plasma membrane CB_1R equilibrium.

Reduced plasma membrane CB_1R levels could provide one explanation for the deficits in basal ERK phosphorylation we observed with CRIP1a over-expression. The fraction of plasma membrane surface CB_1R levels (+/− 15% to 30%) modified over the range of CRIP1a levels examined herein are fairly consistent with the differences in basal ERK phosphorylation observed in these clones (+/− 15% to 30%). In contrast, there was no apparent influence of CRIP1a levels on basal or forskolin-activated cAMP levels. These observations suggest that the pool of plasma membrane CB_1R that participate in constitutive

ERK phosphorylation under the negative influence of CRIP1a, are not involved in constitutive regulation of adenylyl cyclase (type 6 isoform [38]) in N18TG2.

The influence of CRIP1a on agonist-selectivity and the kinetics of increased efficacy of the agonist-driven ERK phosphorylation suggest that there may be alternative underlying mechanism(s) beyond those regulating constitutive activity. Initial (phase I) agonist-driven ERK phosphorylation by CB_1R includes complex interactions with tyrosine kinase receptors, but also regulation of non-receptor src kinases and raf, which require PKA [30]. Thus, this latter regulatory mechanism is intercalated with the CB_1R-mediated inhibition of cAMP via a $G_{i/o}$-mediated mechanism. Both CP55940-mediated inhibition of cAMP accumulation as well as CP55940-driven ERK phosphorylation were enhanced by the reduction in CRIP1a levels. This would be consistent with the thought that endogenous CRIP1a serves to dampen inhibition of cAMP production, thus allowing PKA activity and suppressing maximal ERK phosphorylation (perhaps by increased PKA-mediated phosphorylation, leading to inactive src or raf).

Further evidence from the present studies suggests that additional regulation might be occurring concomitantly: 1) both the CRIP1a KD-augmented component as well as the agonist-driven ERK phosphorylation require a dynamin-dependent process, assumed to be receptor internalization; and 2) the greatest effect of CRIP1a KD was on the ERK1/2 dephosphorylation (aka desensitization), a multistep process that has been shown to involve multiple phosphatases, in phase II of the time-course. Using a HEK cell model, Daigle et al demonstrated that phosphorylation of the CB_1R at Ser426 and Ser430 is required to initiate this “desensitization” phase [40]. We know that phase II is entirely dependent upon CB_1R maintaining PKA in a low activity state, in combination with Ser/Thr PP1-PP2a phosphatase activity, which is speculated to lead to the dephosphorylation and inactivation of MEK [30]. One possible influence of endogenous CRIP1a in phase II might be to facilitate the dephosphorylation of MEK and/or CB_1R, a process that is expected to occur after internalization in recycling endosomes. This scenario would be consistent with the observation that knockdown of CRIP1a enhances ERK phosphorylation downstream of enhanced MEK phosphorylation, such as might be observed in signaling endosomes rather than dephosphorylating recycling endosomes.

CRIP1a can influence CB_1R signaling events occurring at the plasma membrane where G protein and $G\beta\gamma$ activation can initiate PI-3K-mediated transactivation of growth factor receptors, a process required for maximal ERK phosphorylation in N18TG2 cells [30]. We found that reduced CRIP1a expression in KD cells was associated with an increased preference for G_{i3} and G_o interaction with CB_1R. Conversely, the over-expression of CRIP1a strongly reversed this preference so as to attenuate interactions with G_{i3} and G_o in favor of interactions with G_{i1} and G_{i2}. It is noteworthy to mention that CB_1Rs can couple to $G\alpha_{i/o}$ proteins in the absence of exogenous agonists [8,9]. Previous studies, performed using co-immunoprecipitation of CB_1R-G proteins in CHAPS detergent extracts from N18TG2 cells or brain, demonstrated that G_{i3} and G_o association with CB_1R tends to be highly influenced by the CB_1R juxtamembrane C-terminal domain, whereas G_{i1} and G_{i2} association is influenced by 3rd intracellular loop domains [8,9]. One could postulate that the C-terminal interaction with CRIP1a might influence this protein-protein association via

direct steric hindrance, or by interactions with other proteins in a complex that precludes interaction with G_{i3} and G_o.

The switch in $G_{i/o}$ subtype preference might have relevance to cellular signal transduction selectivity. Previous investigations demonstrated that different agonist ligands could disrupt the equilibrium in the association of the CB_1R with different G proteins [10]. For example, WIN55212-2 could promote the dissociation of G_{i1}, G_{i2} and G_{i3} from the immunoprecipitated CB_1R, i.e., serving as a full agonist. In contrast, methanandamide was able to promote dissociation of only G_{i3}, consistent with its behavior as a partial agonist. Our current data support the idea that CRIP1a can influence selectivity by biasing the G protein-CB_1R pool.

Although beyond the scope of this study, it seems probable that CRIP1a could regulate other GPCRs in addition to CB_1R from which its name was derived. The minimal requirement for binding to a sequence at the distal C-terminal of the CB_1R that has relatively limited homology with other GPCRs might limit the likelihood of novel binding partners. However, it is conceivable that the extent of the CRIP1a binding domain might include other domains of the CB_1R intracellular surface that may have greater homology with other proteins, or that other proteins contact CRIP1a via interaction with binding sites different from that of CB_1R. Continued investigation is necessary identify the full functional capabilities of this intriguing small CB_1R-interacting protein.

5. Conclusions

The knowledge gained regarding the effects of CRIP1a on CB_1R signaling demonstrates how CB_1R function and activity can be fine-tuned by accessory proteins. We determined that reduction in CRIP1a protein levels increased CB_1R agonist-stimulated $G_{i3/o}$ protein activation and promoted inhibition of forskolin-stimulated cAMP accumulation in neuroblastoma cells. Depletion of CRIP1a enhanced CB_1R-mediated maximal ERK phosphorylation, a process that was abolished by blocking CB_1R internalization. This loss of function analysis suggests that one role for endogenously expressed CRIP1a may be to promote a CB_1R-$G_{i1/2}$ complex having reduced intrinsic efficacy in response to certain agonist ligands. A complete analysis of the mechanisms involved in CRIP1a regulation of CB_1R signaling can provide additional information on how CB_1R accessory proteins, and specifically CRIP1a, modulate CB_1R activity and the roles these proteins might play in CB_1R-mediated pathologies.

Acknowledgements

This work was supported by US Public Health Services grants: R01-DA03690 (ACH), R21-DA025321 (ACH and DES), K01-DA024763 (CEB), P50-DA006634 (ACH, CEB, KE), K12-GM102773 (KE), T32-DA00724 and F31-DA032215 (LCB).

List of nonstandard abbreviations

2-AG 2-arachidonoylglycerol

BSA	bovine serum albumin
CB_1R	cannabinoid receptor
CP55940	(−)-*cis*-3-[2-Hydroxy-4-(1,1-dimethyl-heptyl)phenyl]-*trans*-4-(3-hydroxypropyl)cyclohexanol
CRIP1a	Cannabinoid Receptor Interacting Protein 1a
DAGL	diacylglycerol lipase
DTT	dithiothreitol
Dynasore	3-Hydroxynaphthalene-2-carboxylic acid (3,4-dihydroxybenzylidene)hydrazide
ERK1/2	extracellular signal-regulated kinases 1 and 2
GPCR	G-protein Coupled Receptor
GRK	G-protein coupled receptor kinase
mAEA	(*R*)-*N*-(2-Hydroxy-1-methylethyl)-5*Z*,8*Z*,11*Z*,14*Z*-eicosatetraenamide
MAPK	mitogen-activated protein kinase
N18TG2	mouse neuroblastoma N18TG2
PBS	phosphate buffered saline
Rp-cAMPs	3′,5′-cyclic monophosphorothioate triethylammonium salt
Sp-cAMPs	Sp-Adenosine 3′,5′-cyclic monophosphorothioate triethylammonium salt hydrate
SR141716	N-(piperidin-1-yl)-5-(4-chlorophenyl)-1-(2,4-dichlorophenyl)-4-methyl-1H-pyrazole-3-carboxamide
THL	tetrahydrolipstatin
WIN55212-2	[2,3-dihydro-5-methyl-3-[(4-morpholinyl)methyl]pyrrolo[1,2,3-de]-1,4-benzoxazin-6-yl](1-naphthyl)methanone

References

[1]. Niehaus JL, Liu Y, Wallis KT, Egertova M, Bhartur SG, Mukhopadhyay S, Shi S, He H, Selley DE, Howlett AC, Elphick MR, Lewis DL. CB1 cannabinoid receptor activity is modulated by the cannabinoid receptor interacting protein CRIP1a. Mol. Pharmacol. 2007; 72:1557–1566. [PubMed: 17895407]

[2]. Eggan SM, Lewis DL. Immunocytochemical distribution of the cannabinoid CB1 receptor in the primate neocortex: a regional and laminar analysis. Cereb. Cortex. 2007; 17:175–191. [PubMed: 16467563]

[3]. Herkenham M, Lynn AB, De Costa BR, Richfield EK. Neuronal localization of cannabinoid receptors in the basal ganglia of the rat. Brain Res. 2001; 547:267–274. [PubMed: 1909204]

[4]. Sim LJ, Hampson RE, Deadwyler SA, Childers SR. Effects of chronic treatment with delta9-tetrahydrocannabinol on cannabinoid-stimulated [35S]GTPgammaS autoradiography in rat brain. J. Neurosci. 1996; 16:8057–8066. [PubMed: 8987831]

[5]. Pertwee RG. The pharmacology of cannabinoid receptors and their ligands: an overview. Int. J. Obes. (Lond). 2006; 30:S13–S18. [PubMed: 16570099]

[6]. Seely KA, Prather PL, James LP, Moran JH. Marijuana-based drugs: innovative therapeutics or designer drugs of abuse? Mol. Interv. 2011; 11:36–51. [PubMed: 21441120]

[7]. Howlett AC. Cannabinoid receptor signaling. Handbook of Experimental Pharmacology. 2005:53–79. [PubMed: 16596771]

[8]. Mukhopadhyay S, McIntosh HH, Houston DB, Howlett AC. The CB(1) cannabinoid receptor juxtamembrane C-terminal peptide confers activation to specific G proteins in brain. Mol. Pharmacol. 2000; 57:162–170. [PubMed: 10617691]

[9]. Mukhopadhyay S, Howlett AC. CB1 receptor-G protein association. Subtype selectivity is determined by distinct intracellular domains. Eur. J. Biochem. 2001; 268:499–505. [PubMed: 11168387]

[10]. Mukhopadhyay S, Howlett AC. Chemically distinct ligands promote differential CB1 cannabinoid receptor-Gi protein interactions. Mol. Pharmacol. 2005; 67:2016–2024. [PubMed: 15749995]

[11]. Howlett AC, Blume LC, Dalton GD. CB1 Cannabinoid Receptors and their Associated Proteins. Curr Med Chem. 2010; 17:1382–1393. [PubMed: 20166926]

[12]. Smith TH, Sim-Selley LJ, Selley DE. Cannabinoid CB1 receptor-interacting proteins: novel targets for central nervous system drug discovery. Br. J. Pharmacol. 2010; 160:454–466. [PubMed: 20590557]

[13]. Stauffer B, Wallis KT, Wilson SP, Egertova M, Elphick MR, Lewis DL, Hardy LR. CRIP1a switches cannabinoid receptor agonist/antagonist-mediated protection from glutamate excitotoxicity. Neurosci. Lett. 2011; 503:224–228. [PubMed: 21896317]

[14]. Selley DE, Jacob JC, Smith TH, Blume LC, Shim H, Straiker A, Mackie K, Howlett AC, Sim-Selley LJ, Chen C. Functional characterization of cannabinoir receptor-interacting protein CRIP1a. FASEB J. 2013; 27:882.4. [PubMed: 23193173]

[15]. Blume, LC.; Eldeeb, KM.; Howlett, AC. Wiley-Blackwell Publications; 2014. Cannabinoid Receptor Intracellular Signaling: the Long Journey from Binding Sites to Biological Effects, Chapter 2, Cannabinoids: Fifty Years of Research.

[16]. Bisogno T, Howell F, Williams G, Minassi A, Cascio MG, Ligresti A, Matias I, Schiano-Moriello A, Paul P, Williams EJ, Gangadharan U, Hobbs C, Di Marzo V, Doherty P. Cloning of the first sn1-DAG lipases points to the spatial and temporal regulation of endocannabinoid signaling in the brain. J. Cell. Biol. 2003; 163:463–468. [PubMed: 14610053]

[17]. Blume LC, Bass CE, Childers SR, Dalton GD, Roberts DC, C. D, Richardson JM, Xiao R, Selley DE, Howlett AC. Striatal CB1 and D2 receptors regulate expression of each other, CRIP1A and delta opioid systems. J. Neurochem. 2013; 124:808–820. [PubMed: 23286559]

[18]. Wacker JL, Feller DB, Tang X, DeFino MC, Namkung Y, Lyssand JS, Mhyre AJ, Tan X, Jensen JB, Hague C. Disease-causing mutation in GPR54 reveals the importance of the second intracellular loop for class A G-protein-coupled receptor function. J. Biol. Chem. 2008:31068–31078. [PubMed: 18772143]

[19]. Howlett AC, Fleming RM. Cannabinoid inhibition of adenylate cyclase. Pharmacology of the response in neuroblastoma cell membranes. Mol. Pharm. 1984; 26:532–538.

[20]. Meschler JP, Kraichely DM, Wilken GH, Howlett AC. Inverse agonist properties of N-(Piperidin-1-yl)-5-(4-chlorophenyl)-1-(2,4 dichlorophenyl)-4-methyl-1H-pyrazole-3-carboxamide (SR141716A) and 1-(2-chlorophenyl)-4-cyano-5-4(4-methoxyphenyl)-1H-pyrazolone-3-carboxylic acid phenylamide (CP-272871) for the CB1 cannabinoid receptor. Biochem. Pharmacol. 2000; 69:1315–1323. [PubMed: 11008125]

[21]. Eldeeb K, Leone-Kabler S, Blume LC, Howlett AC. CB1 receptor intracellular loop 4 mutation modulates G protein activation and camp production in human neuroblastoma cells. Annual Symposium on the Cannabinoids. 2014; 24:50.

[22]. Leterrier C, Bonnard D, Carrel D, Rossier J, Lenkei Z. Constitutive endocytic cycle of the CB1 cannabinoid receptor. J. Bio. Chem. 2004; 279:36013–36021. [PubMed: 15210689]

[23]. McDonald NA, Henstridge CM, Connolly CN, Irving AJ. An essential role for constitutive endocytosis, but not activity, in the axonal targeting of the CB1 cannabinoid receptor. Mol. Pharmacol. 2007; 71:976–984. [PubMed: 17182888]

[24]. Rinaldi-Carmona M, Le Duigou A, Oustric D, Barth F, Bouboula M, Carayon P, Casellas P, Le Fur G. Modulation of CB1 cannabinoid receptor functions after a long-term exposure to agonist or inverse agonist in the chinese hamster ovary cell expression system. J. Pharmacol. Exp. Ther. 1998; 287:1038–1047. [PubMed: 9864290]

[25]. Marazzi J, Kleyer J, Paredes JM, Gertsch J. Endocannabinoid content in fetal bovine sera - unexpected effects on mononuclear cells and osteoclastogenesis. J. Immunol. Methods. 2011; 373:219–228. [PubMed: 21920367]

[26]. Blume LC, Bass CE, Dalton GD, Selley DE, Howlett AC. Cannabinoid Receptor Interacting Protein (CRIP1a) modulates CB1 receptor trafficking, activity, and signaling. Annual Symposium on the Cannabinoids. 2012; 22:26.

[27]. Sarnataro D, Grimaldi C, Pisanti S, Gazzerro P, Laezza C, Zurzolo C, Bifulco M. Plasma membrane and lysosomal localization of CB1 cannabinoid receptor are dependent on lipid rafts and regulated by anandamide in human breast cancer cells. FEBS Lett. 2005; 579:6343–6349. [PubMed: 16263116]

[28]. Bari M, Battista N, Fezza F, Finazzi-Agro A, Maccarrone M. Lipid rafts control signaling of type-1 cannabinoid receptors in neuronal cells. Implications for anandamide-induced apoptosis. J. Biol. Chem. 2005; 280:12212–12220. [PubMed: 15657045]

[29]. Bari M, Oddi S, De Simone C, Spagnolo P, Gasperi V, Battista N, Centonze D, Maccarrone M. Type-1 cannabinoid receptors colocalize with caveolin-1 in neuronal cells. Neuropharmacology. 2008; 54:45–50. [PubMed: 17714745]

[30]. Dalton GD, Howlett AC. Cannabinoid CB1 receptors transactivate multiple receptor tyrosine kinases and regulate serine/threonine kinases to activate ERK in neuronal cells. Br. J. Pharmacol. 2012; 165:2497–2511. [PubMed: 21518335]

[31]. Howlett AC, Qualy JM, Khachatrian LL. Involvement of Gi in the inhibition of adenylate cyclase by cannabimimetic drugs. Mol. Pharmacol. 1986; 29:307–313. [PubMed: 2869405]

[32]. Mukhopadhyay S, Shim JY, Assi AA, Norford D, Howlett AC. CB(1) cannabinoid receptor-G protein association: a possible mechanism for differential signaling. Chem. Phys. Lipids. 2002; 121:91–109. [PubMed: 12505694]

[33]. Hu SS, Arnold A, Hutchens JM, Radicke J, Cravatt BF, Wager-Miller J, Mackie K, Straiker A. Architecture of cannabinoid signaling in mouse retina. J. Comp. Neurol. 2010; 518:3848–3866. [PubMed: 20653038]

[34]. Fernandez-Ruiz J, Hernandez M, Ramos JA. Cannabinoid-dopamine interaction in the pathophysiology and treatment of CNS disorders. CNS Neurosci. Ther. 2010; 16:72–91.

[35]. Dalton GD, Bass CE, Van Horn CG, Howlett AC. Signal transduction via cannabinoid receptors. CNS Neurol. Disord. Drug Targets. 2009; 8:422–431. [PubMed: 19839935]

[36]. Turu G, Hunyady L. Signal transduction of the CB1 cannabinoid receptor. J. Mol. Endocrinol. 2010; 44:75–85. [PubMed: 19620237]

[37]. Leterrier C, Laine J, Darmon M, Boudin H, Rossier J, Lenkei Z. Constitutive activation drives compartment-selective endocytosis and axonal targeting of type 1 cannabinoid receptors. J. Neurosci. 2006; 26:3141–3153. [PubMed: 16554465]

[38]. McVey M, Hill J, Howlett AC, Klein C. Adenylyl cyclase, a coincidence detector for nitric oxide. J. Biol. Chem. 1999; 274:18887–18892. [PubMed: 10383385]

[39]. Dalton GD, Howlett AC. Cannabinoid CB1 receptors transactivate multiple receptor tyrosine kinases and regulate serine/threonine kinases to activate ERK in neuronal cells. Br. J. Pharmacol. 2012; 165:2497–2511. [PubMed: 21518335]

[40]. Daigle TL, Kwok ML, Mackie K. Regulation of CB1 cannabinoid receptor internalization by a promiscuous phosphorylation-dependent mechanism. J. Neurochem. 2008; 106:70–82. [PubMed: 18331587]

Highlights

- Cannabinoid Receptor Interacting Protein 1a (CRIP1a) decreases CB1R at the plasma membrane surface without altering total CB1R mRNA or protein levels in a neuronal cell model.
- CRIP1a regulates both constitutive and agonist-stimulated extracellular signal-regulated kinase phosphorylation in a neuronal cell model.
- CRIP1a regulates inhibition of cyclic AMP accumulation.
- CRIP1a switches the subtype preference for Gi/o proteins.
- These are the first demonstrations of cellular functional responses modulated by the abundance of CRIP1a in a neuronal cell.

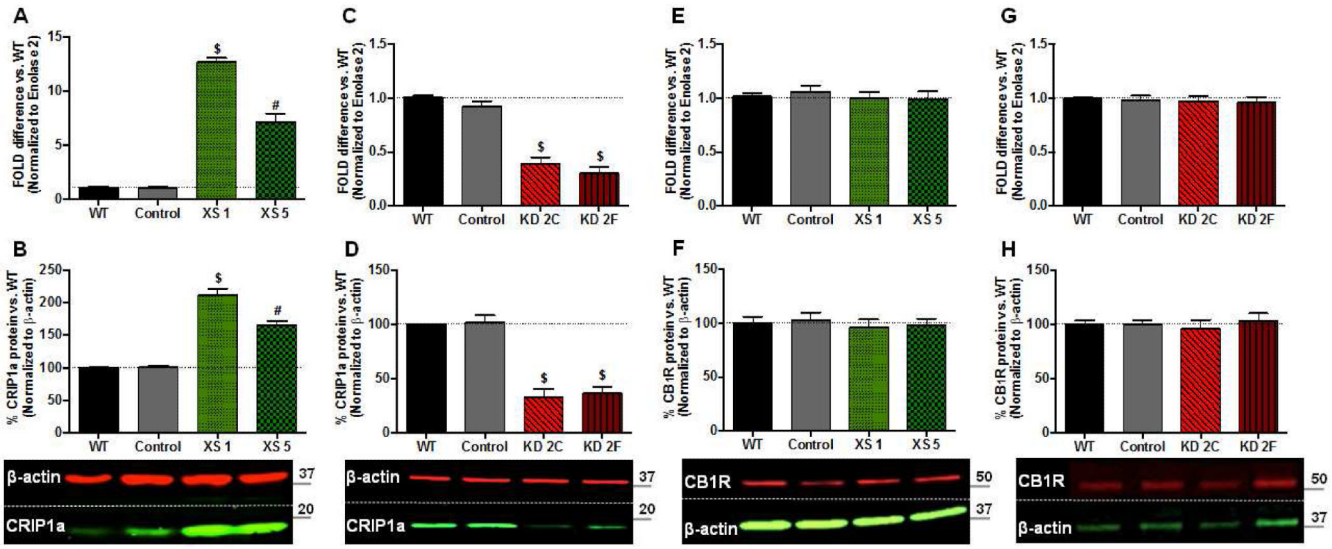

Figure 1. Stable transgenic CRIP1a over-expressing (XS) and knockdown (KD) clones do not alter CB_1 receptor expression

A,*C*,*E*,*G*: N18TG2 WT, empty vector (Control), CRIP1a XS (*A*,*E*), and CRIP1a KD cells (*C*,*G*) were subjected to qPCR to quantitate mRNA levels of CRIP1a (*A*, *C*) and CB_1R (*E*,*G*). ΔΔCt values are expressed as the fold-difference from WT, represented as 1. *B*,*D*,*F*,*H*: Protein levels were determined by Western blots of whole cell lysates from N18TG2 WT, empty vector (Control), CRIP1a XS (*B*,*F*), and CRIP1a KD cells (*D*,*H*). The band density ratio of CRIP1a:β-actin (*B*,*D*) or CB_1R:β-actin (*F*,*H*) were calculated for each individual clone, and normalized to WT as 100%. Below, representative Western blots are shown. Data are expressed as the mean ± S.E.M. from six independent experiments. $^{\#}p<0.01$, $^{\$}p<0.001$ indicates significant difference from WT using Student's *t* test.

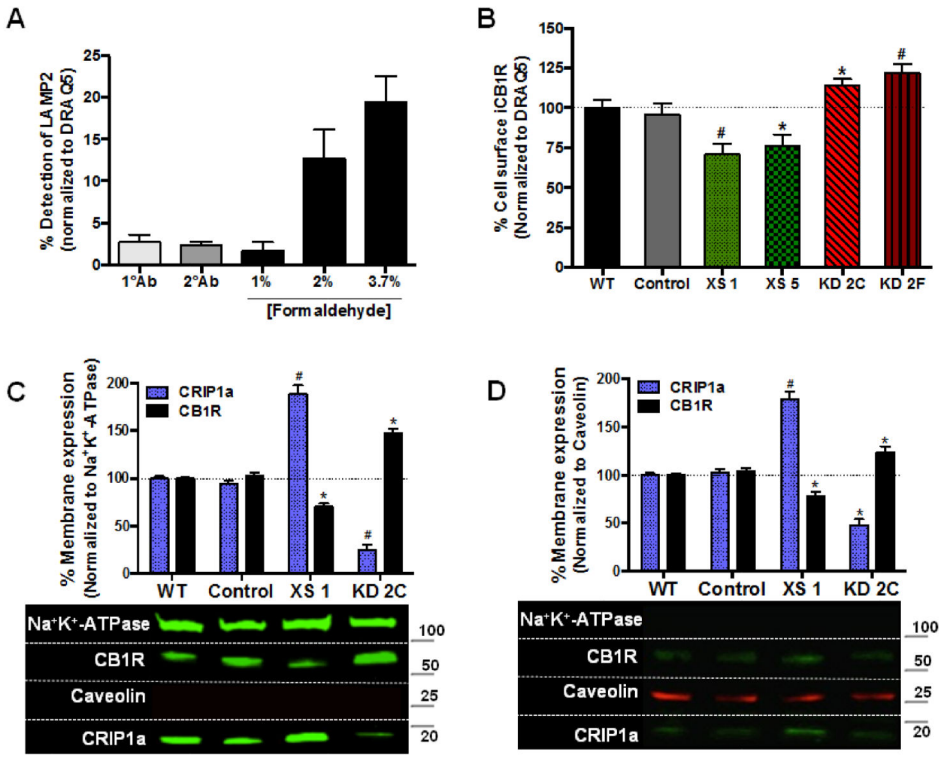

Figure 2. CRIP1a alters CB_1R cell surface equilibrium

(*A*) On-cell-Western technique recognizes extracellular epitope of the CB_1R on the plasma membrane, but does not recognize extracellular epitopes within internalized vesicles. N18 WT cells were plated and grown until 90% confluent in a 96-well plate, serum-starved for 16 h, and then treated for 2 h with 1 μM THL to attenuate the production of 2-AG. Cells were fixed with 1%, 2%, or 3.7% of ice-cold phosphate-buffered formalin at 21-23°C for 15 min to determine a formalin concentration capable of fixing the cells without altering plasma membrane permeability. Cells were washed with PBS then incubated at 4°C overnight with a primary antibody recognizing LAMP2, a luminal endosomal marker or an IgG isotype control goat antibody. LAMP2 was used as a positive control for determining the extent of cell permeabilization, and the IgG isotype was used as a negative control to account for background and non-specific immunobinding. Cells were washed, incubated with an IR-conjugated secondary antibody, and then stained with the nuclear marker DRAQ5 to account for well-to-well variations in cell number. Quantitation of LAMP2 was calculated as the ratio of immunoreactive LAMP2:DRAQ5. (*B*) N18TG2 WT, empty vector (Control), CRIP1a XS and CRIP1a KD cells were subjected to the On-cell-Western assay, as described above using 1.2% ice-cold phosphate-buffered formalin fixative. Calculation of CB_1R surface expression was determined as the ratio of immunoreactive CB_1R:DRAQ5, and compared to WT set as 100%. (*C,D*) Cell membranes were fractionated and Western blots of NP-40 soluble (*C*) and NP-40-resistant (*D*) membrane lysates were probed for Na^+K^+-ATPase and caveolin to identify fractions containing plasma membrane and lipid rafts, respectively. Below, representative Western blots are shown. Data are expressed as the mean

± S.E.M. from six (*A* and *B)* and three (*C* and *D*) independent experiments.
*p<0.05, #p<0.01 indicates significant difference from WT using Student's *t* test.

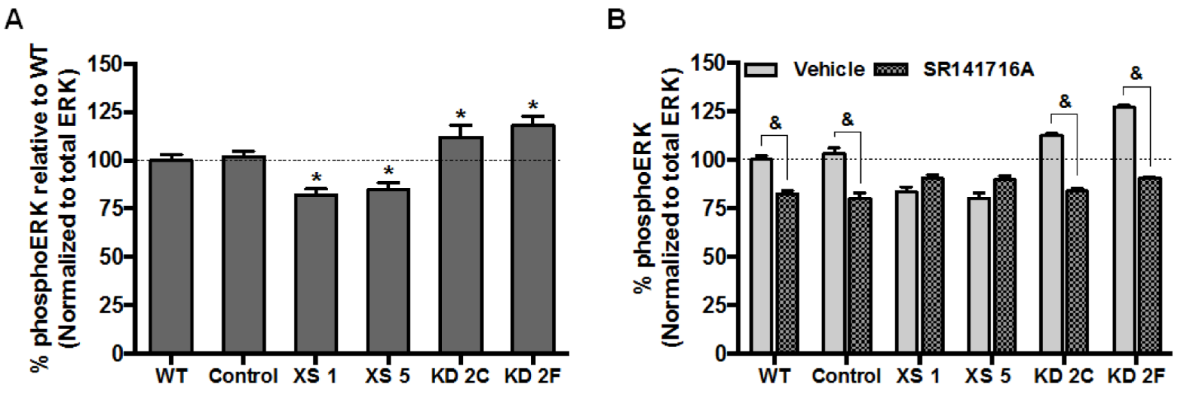

Figure 3. CRIP1a modulates CB_1R-mediated non-ligand dependent constitutive phosphoERK1/2

(*A*) N18TG2 WT, empty vector (Control), CRIP1a XS, and CRIP1a KD cells were serum-starved for 16 h, pretreated for 2 h with 1 μM THL, and quantitated for non-ligand mediated CB_1R constitutive phosphoERK1/2 using the In-cell-Western assay as described in Materials and Methods. To determine phosphoERK levels the ratio of immunoreactive phosphoERK:ERK was calculated for each individual clone and compared to WT set as 100%. (*B*) Cells were serum-starved for 16 h, pretreated for 2 h with 1 μM THL, and treated with either vehicle or 10 nM of the CB_1R antagonist SR141716A for 5 min. PhosphoERK1/2 was calculated as the ratio of phosphoERK1/2 to total ERK, and compared to WT basal levels, set as 100%. Data are expressed as the mean ± S.E.M. from four independent experiments performed in duplicate. & $p<0.05$ indicates significantly different from vehicle, and *$p<0.05$ indicates significantly different from WT using one-way ANOVA and Dunnett's post-hoc test.

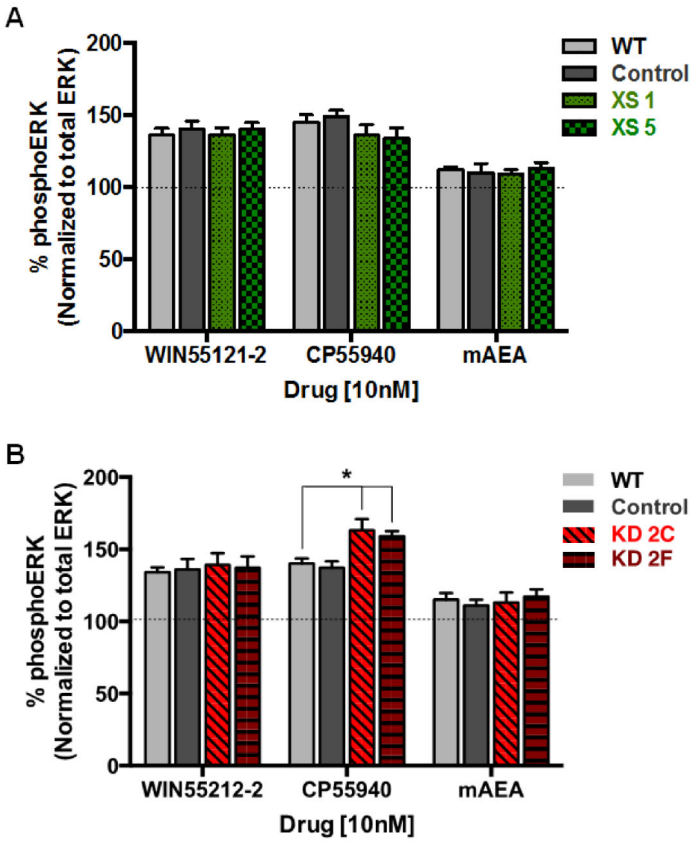

Figure 4. Influence of CRIP1a on CB_1R agonist-mediated ERK1/2 phosphorylation

(*A* and *B*) N18TG2 WT, empty vector (Control), CRIP1a XS (*A*), and CRIP1a KD (*B*) cells were serum-starved for 16 h, pretreated for 2 h with 1 μM THL, and treated with either vehicle, the CB_1R full agonist WIN55212-2 (10 nM), CP55940 (10 nM), or the CB_1R partial agonist mAEA (10 nM) for 5 min. Immunoreactive phosphoERK1/2 was determined using the In-cell-Western assay as described in the Materials and Methods. Quantitation of phosphoERK1/2 was calculated as the ratio of immunoreactive phosphoERK1/2 to total ERK, and compared to basal, represented as 100% for each clone. *Indicates significantly different from WT CP55940 treated using one-way ANOVA and Dunnett's post-hoc test ($F_{3,16}$=6.36, p<0.05).

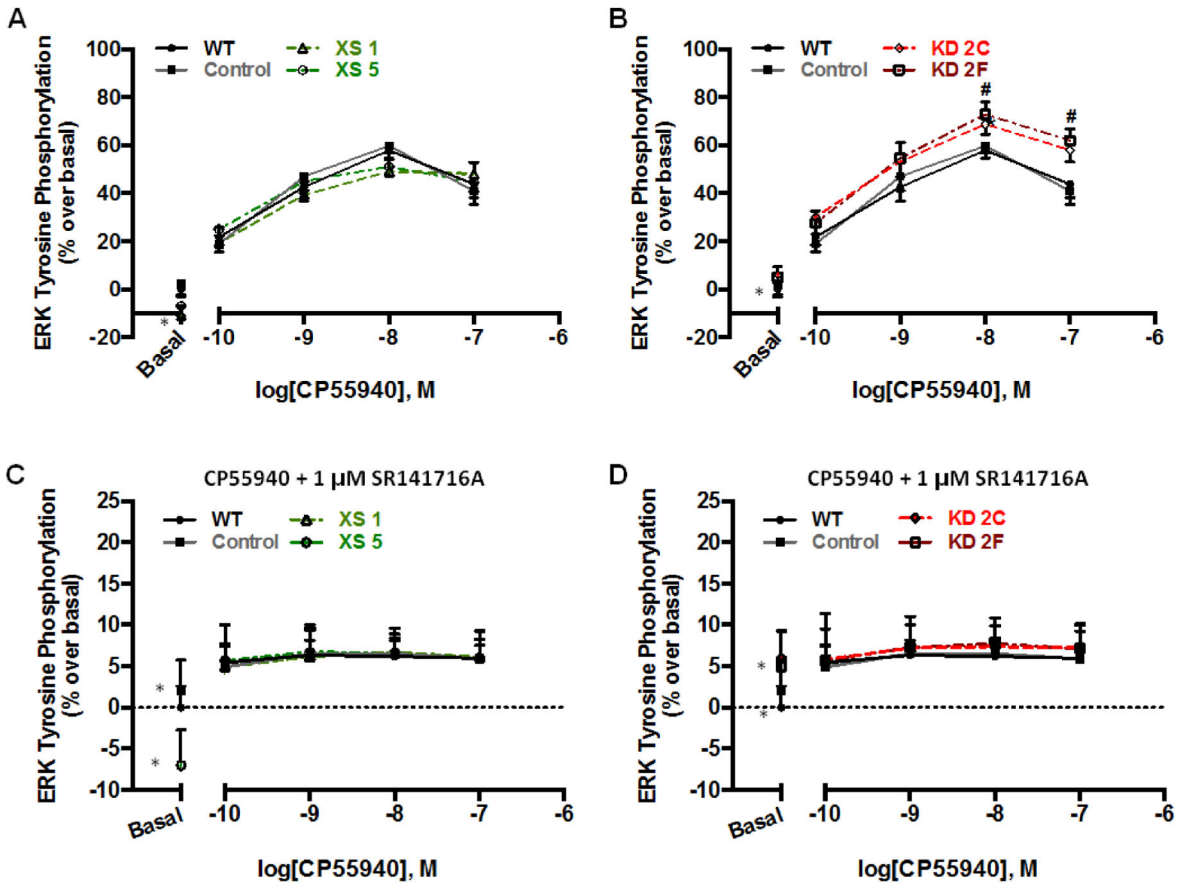

Figure 5. Efficacy of CP55940-stimulated phosphoERK1/2 is enhanced by depletion of CRIP1a

N18TG2 WT, empty vector (Control), CRIP1a XS (*A*,*C*), and CRIP1a KD (*B*,*D*) cells were serum-starved for 16 h, pretreated for 2 h with 1 μM THL, and treated with varying concentrations of CP55940 (*A*,*B*), or CP55940 in the presence of 1 μM SR141716A (*C*,*D*) for 5 min. In-cell-Western analysis of phosphoERK1/2 was quantified as the ratio of phosphoERK1/2:total ERK, and then phosphoERK values were presented as a percent change relative to basal for each clone. Data are presented as the mean ± S.E.M. calculated from three independent experiments performed in duplicate. #$p<0.05$ indicates that data points significantly differ from WT, using a two-way ANOVA and Bonferroni post-hoc test. *A significant difference from basal was observed for CRIP1a XS and KD clones, as indicated in Fig. 1*A*, *B*, *C* and *D*, respectively.

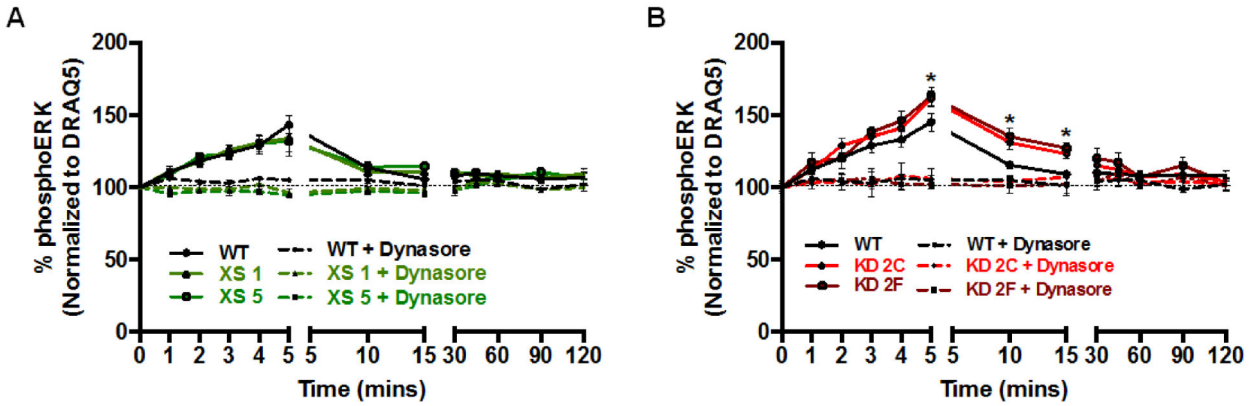

Figure 6. Effect of CRIP1a on the kinetics of ERK1/2 phosphorylation

N18TG2 WT and CRIP1a XS (*A*) and N18TG2 WT and CRIP1a KD clones (*B*) were serum starved for 16 h, treated with THL for 2 h, and pretreated for 30 min in the absence or presence of the dynamin inhibitor Dynasore (80 μM), and then challenged with the CB_1R agonist CP55940 (10 nM) for the indicated times. PhosphoERK1/2 levels were determined as the ratio of immunoreactive phosphoERK1/2:DRAQ5. PhosphoERK values were represented as a percent change relative to basal, expressed as 100% for WT cells. No significant differences in total ERK levels from time 0 were detected in time course data for untreated or Dynasore-treated cells (data not shown). Data are presented as the mean ± S.E.M. from four independent experiments performed in duplicate. *$p<0.05$ indicates significant difference from WT using a two-way ANOVA and Bonferroni post-hoc.

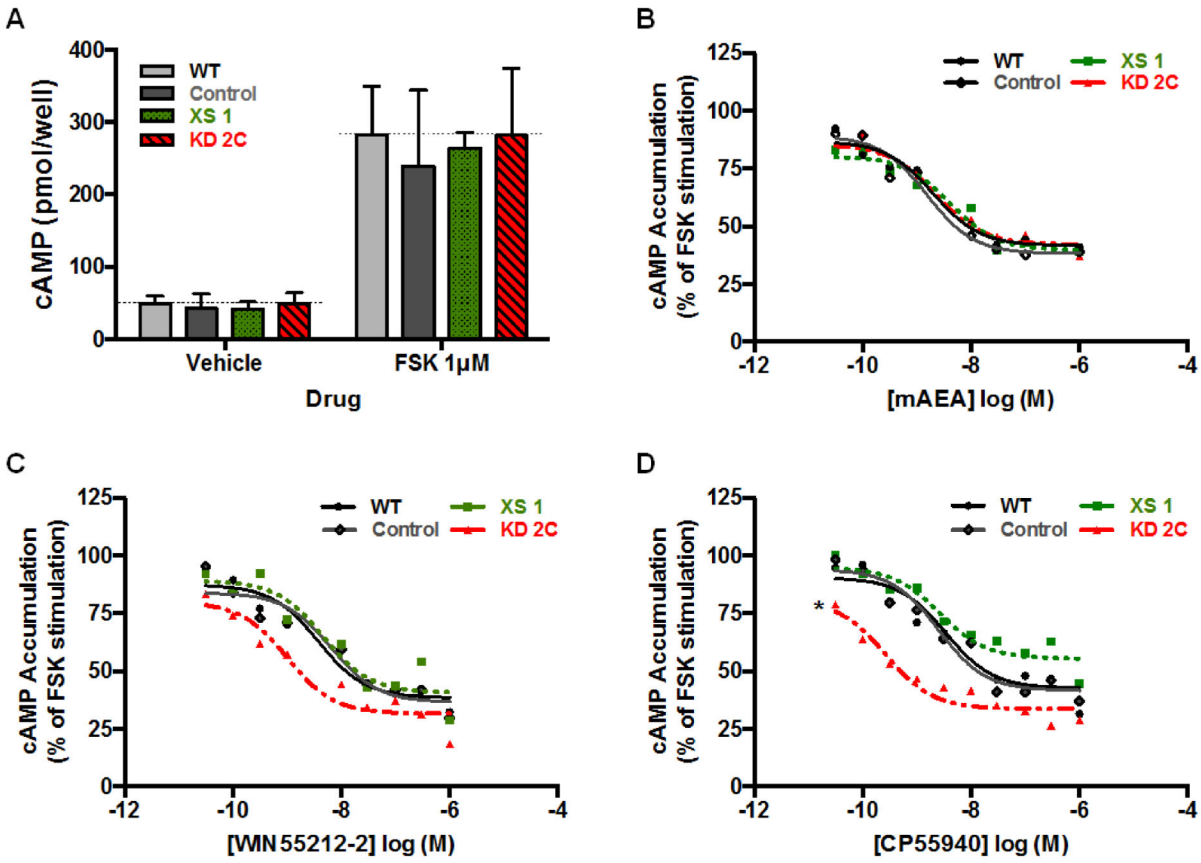

Figure 7. Effects of CRIP1a on CB_1R-mediated inhibition of cAMP accumulation

(*A*) cAMP levels in WT, empty vector Control, and XS or KD clones were determined by incubating cells with vehicle or 1 μM forskolin for 4 min (a time within the linear range of stimulation). (*B-D*) Dose-response curves for cannabinoid agonist inhibition of cAMP accumulation, using forskolin as an adenylyl cyclase activator, was determined in N18TG2 WT, Control vector, CRIP1a XS, and CRIP1a KD cells with either mAEA (*B*), WIN55212-2 (*C*), or CP55940 (*D*). Background levels (cAMP accumulation in the absence of FSK) were subtracted from all values and represented less than 10% of FSK-stimulated cAMP accumulation (*A*). Data were normalized such that 100% was equal to cAMP in WT cells treated with forskolin only, while 0% was equal to cAMP in cells treated with vehicle only. *$p<0.05$ indicates significant difference between WT and CRIP1a KD in the EC_{50} values calculated from nonlinear regression fitting of CP55940 concentration-effect curves and two-way ANOVA.

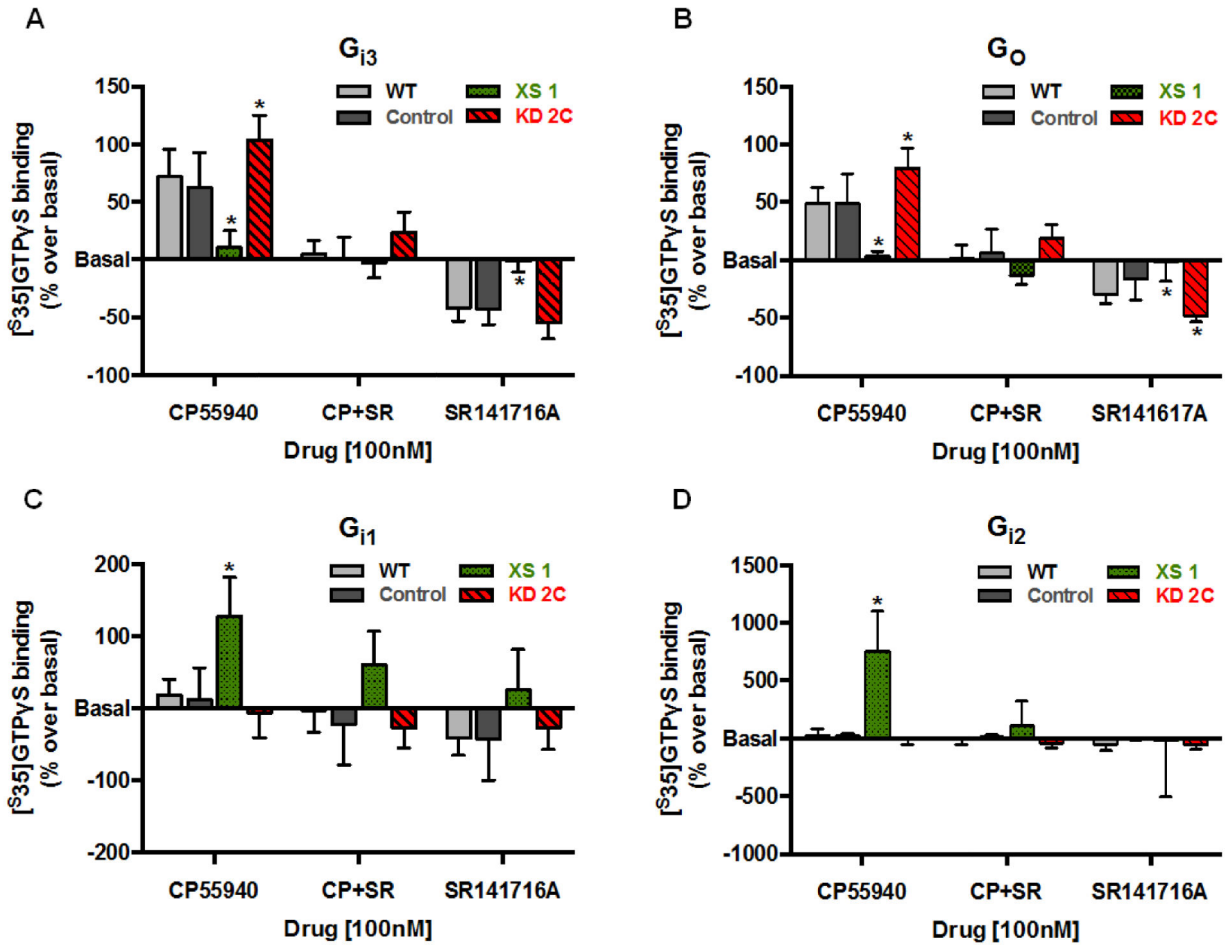

Figure 8. Effects of CRIP1a on CB_1-regulated [^{35}S]GTPγS binding to $G_{i/o}$ proteins

Membranes from N18TG2 WT, empty vector (Control), CRIP1a XS, or CRIP1a KD cells were incubated with 100 mM NaCl, 10 μM GDP, 500 pM [^{35}S]GTPγS and either 100 nM CP55940, 100 nM SR141716A, or co-incubated with 100 nM CP55940 plus SR141716A. Membranes were then subjected to immunoselective scintillation proximity assay to quantitate ligand-mediated coupling to either $G\alpha_{i3}$ (*A*), $G\alpha_o$ (*B*), $G\alpha_{i1}$, or $G\alpha_{i2}$ (*C*) as described in Materials and Methods. Ligand-stimulated values were transformed to "percent over/under basal" [% = (stimulated-basal)/(basal)*100]. Data are shown as the mean ± S.E.M. values of five or more independent experiments performed in duplicate. *Indicates significant difference from WT using one-way ANOVA (A: $F_{3,16}$=10.05); B: $F_{3,16}$=12.42;) and Dunnett's post-hoc test ($p<0.05$).